RSC Advances

ROYAL SOCIETY OF CHEMISTRY

www.rsc.org/advances

RSC Advances

RSCPublishing

ARTICLE

Preparation and characteristics of molecularly homogeneous Ag/AgCl nano-heterostructures via two-step synthesis

Cite this: DOI: 10.1039/x0xx00000x

Received 00th January 2012,
Accepted 00th January 2012

DOI: 10.1039/x0xx00000x

www.rsc.org/

Ping Yang,[a*] Changchao Jia,[a] Haiyan He,[a] Ling Chen[a] and Katarzyna Matras-Postolek[b]

Ag/AgCl nano heterostructures with different degrees of molecular homogeneity and high photocatalytic activity have been created through a two-step synthesis in ethanol via a oxidation route in situ at room temperature. The result offers an alternative method for synthesizing molecular homogeneous metal/semiconductor nanocomposites. The heterostructures with AgCl ratios of 50 and 80% revealed excellent performance for the photocatalytic degradation of methyl orange molecules. This technique had the advantages of convenient operation, low cost, and mass production and built up a great molecularly homogeneous composite structure of Ag/AgCl which exhibited high photocatalytic activity and stability towards the decomposition of organic methyl orange.

Introduction

Photocatalysis is accelerating a photoreaction in the presence of a catalyst and is becoming promising in many applications with the utilization of solar energy.[1] In recent years, attentions have been paid to design Ag/AgX (X = Cl, Br, I) composite materials due to the surface Plasmon resonance (SPR) of metallic Ag and their excellent photocatalytic activity and high stability.[2,3] Efficient and stable visible-light driven Ag@AgCl (or Ag@AgBr) photocatalysts have been fabricated through a direct reaction between $AgNO_3$ and HCl followed by converting some Ag^+ ions to Ag^0 species via UV irradiation or through an ion-exchange reaction between the aqueous solution of Ag_2MoO_4 and HCl (or HBr).[4-8] Hierarchical porous AgCl@Ag hollow architectures revealed highly enhanced visible light photocatalytic activity.[9-12] Furthermore, both highly photocatalysis behavior and yields are important for research and applications.

Ag/AgCl nano heterostructures exhibit an ideal performance in photocatalysis. Regular nano heterostructures such as nanowires and cubes revealed highly photolysis activity. However, these nanomaterials have to be fabricated using a complex procedure with low yields,[1,2,9] which significantly limits their practical applications. In addition, Ag/AgCl heterostructures with different morphologies have been synthesized in recent years.[13-15] For example, Chen and co-workers reported cube-like Ag/AgCl structures fabricated from sodium chloride and silver acetate for highly efficient sunlight-driven photocatalysts.[13] Cube-like Ag/AgCl was created using CH_2Cl_2 to slow release chloride source.[14] To improve the photocatalytic activity, Liu et al. fabricated Ag/AgCl heterostructures using graphene oxide as a capping agent to adjust the size and shape and increase surface area for enhancing visible light photocatalytic performance. Although these heterostructures revealed high photocatalysis activity, a limitation still retained for applications because of the difficulty of the controlling of preparation process. There is an urgent need to find a simple and facile method to synthesize Ag/AgCl nano heterostructures for improving their performance and applications.

It is well known, an ideal photocatalysis material has three basic features including fast migration rate of charge carrier, efficient separation of photo generated electron–hole pairs, and a large specific surface area. Recent advances in plasmonic photocatalysis have revealed that integrated plasmonic metal nanostructures generating local electro-magnetic-fields allow efficient separation of photo-induced electron–hole.[16] To increase the surface areas of AgX-based photocatalysts, a variety of spherical, cubic, one-dimensional, and porous nanostructures have been fabricated by using various synthetic routes.[17] Ag/AgCl nano heterostructures revealed a high photocatalytic performance in UV and visible-light regions for the photo degradation of methylorange (MO). Previous studies have been reported that heterostructures was created from Ag nanowires with a single crystalline structure for the fast migration rate of the charge carrier.[18] Such heterostructure exhibited a high photocatalytic activity due to their uniform component distribution of Ag and AgCl. In addition, these materials with regular morphologies request special preparation procedure which limited their applications. There were very few reports for Ag/AgCl nano heterostructures regarding its molecular homogeneity and microstructure.

Herein, we have reported a two-step synthesis to fabricate molecularly homogeneous Ag/AgCl nano heterostructures as highly efficient photocatalysis which can drive degradation of organics. Moreover, it has been found that the morphology of the Ag/AgCl heterostructure is different in that of Ag particles. The components of the obtained heterostructures can be easily controlled by adjusting the feeding amount of $FeCl_3$ in solutions. The morphology, size, and photocatalytic activity of samples depended strongly on their compositions. The Ag/AgCl heterostructures prepared using AgCl/Ag molar ratios of 50 and 80% revealed great photocatalytic behavior. Because of facial synthesis, enhanced photolysis performance, and high yield, this result is utilizable for practical

applications.

Experimental

Synthesis of samples

All of the chemicals used in this work were of analytical reagent grade. For the synthesis of Ag/AgCl nanoheterotructures, typically, $AgNO_3$ of 0.08 g was dissolved in 20 mL of ethanol. Meanwhile, NaOH of 0.03 g was dissolved in 20 mL of ethanol. The ethanol solution of NaOH was added into the ethanol solution of $AgNO_3$ drop by drop with stirring. Sometime later, loose Ag particles (sample 1) were prepared. The $FeCl_3$ ethanol solution of 10 mL was injected into the above-mentioned solution of the Ag particles with certain feeding rates. The mixture was stirred for 3 h to ensure the reaction carried out completely. The resulting samples were rinsed with de-ionized water (resistivity ~ 18 MΩ·cm) and centrifuged at 4000 rpm to remove unreacted chemicals. The preparation conditions of Ag/AgCl loose heterostructures (samples 2-9) were illustrated in Table 1.

Table 1 Preparation conditions of Ag/AgCl heterostructures and rate constant *k* of MO decomposition reaction.

Sample	AgCl molar ratio (%)	Reaction rate constant *k*
1	0	N/A
2	10	0.0009
3	30	0.0016
4	50	0.0824
5	60	0.0159
6	70	0.0250
7	80	0.0810
8	90	0.0107
9	100	0.0207

Characterization

The phase composition of samples was identified by using an X-ray diffractormeter (Bruker D8-Advance, Germany). The morphologies and sizes of samples were taken on a field-emission scanning electron microscope (FESEM, QUANTA 250 FEG, FEI, USA). N_2 adsorption-desorption isotherms were obtained at liquid nitrogen temperature (77 K) using a multi-function adsorption instrument (MFA-140 of Beijing Builder company). Specific surface area was calculated by the Brunaur-Emmett-Teller (BET) method using the adsorption data at the range from $P/P_0 = 0.05$ to 0.35 just below the capillary condensation, and the pore diameter distribution curve was derived from the desorption branch by the BJH method.

Photocatalytic tests

The aqueous solution of methyl orange (MO) was used as target pollutants to evaluate the Ag/AgCl nano heterostructures with different AgCl under ultravilolet (UV) light irradiation. 0.01 g of photocatalyst was used for the degradation of 20 mL MO solution (10 mM) under a (12 W) UV light. The distance between the target solution and the lamp was 30 cm. Before irradiation, samples were stirred for 30 min in dark to make sure the adsorption equilibrium. 2 mL of solution was taken out from the test sample every a certain time. The absorption spectra of samples were recorded by a conventional UV-Vis spectrometer (Hitachi U-4100).

Results and discussion

A two-step synthesis was used for creating Ag/AgCl nano heterostructures as demonstrated in Scheme 1. Ag particles were firstly prepared through the reaction of $AgNO_3$ and NaOH in ethanol. The oxidization of Ag into Ag^+ ions by Fe^{3+} ions then occurred and combined with Cl^- ions to form AgCl immediately. The reaction is below.

$$Ag + Fe^{3+} + Cl^- \rightarrow Fe^{2+} + AgCl\downarrow$$

The half reactions are:

$$Ag + Cl^- \rightarrow AgCl\downarrow + e \quad (E^{\theta}_{AgCl/Ag} = +0.223\ V)$$

$$Fe^{3+} + e \rightarrow Fe^{2+} \qquad (E^{\theta}_{Fe^{3+}/Fe^{2+}} = +0.771\ V)$$

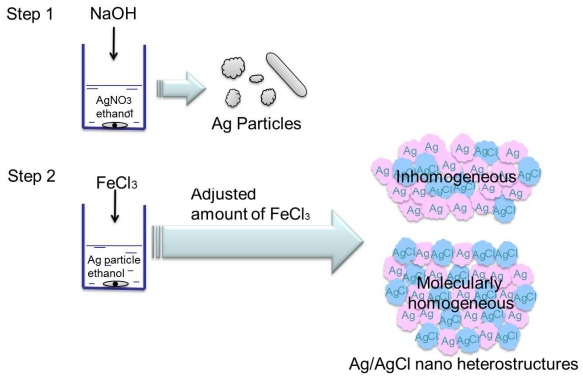

Scheme 1 Preparation procedure of Ag/AgCl heterostructures.

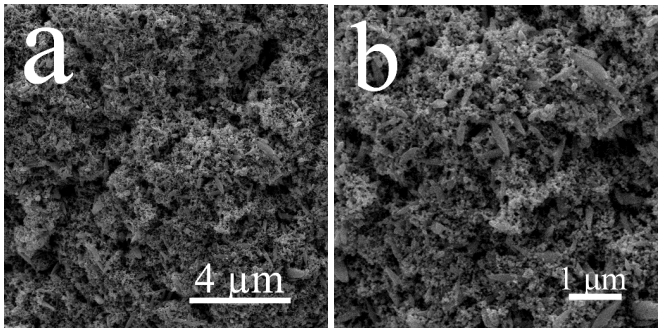

Fig. 1 SEM images of as-prepared Ag particles (sample 1). (a) and (b) Same specimen under different magnification.

Table 1 shows the composition of samples. Fig. 1 shows the scanning electron microscopy (SEM) images of as-prepared Ag particles (sample 1 as illustrated in table 1). The Ag particles revealed two morphologies including irregular particles and long rods as shown in Fig. 1a and 1b. To confirm the formation of Ag phase, Fig. 2 shows the X-ray diffraction (XRD) pattern of sample 1. All of XRD peaks in Fig. 2 matched with those of Ag materials. This indicates single Ag phase was obtained although two morphologies were observed. When the solution of NaOH was dropped into the ethanol solution of Ag^+, the nucleation and growth of Ag occurred because of a quick

reaction rate. Because silver seeds (single and multiple crystalline) with a variety of crystal structure might be produced in the initial stage, finally two morphologies of irregular particles and long rods were created. In practically, inhomogeneous nucleation and growth resulted in large Ag rod formed as shown in Fig. 1b.

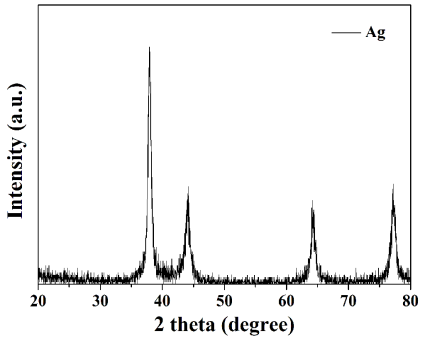

Fig. 2 XRD pattern of Ag particles (sample 1).

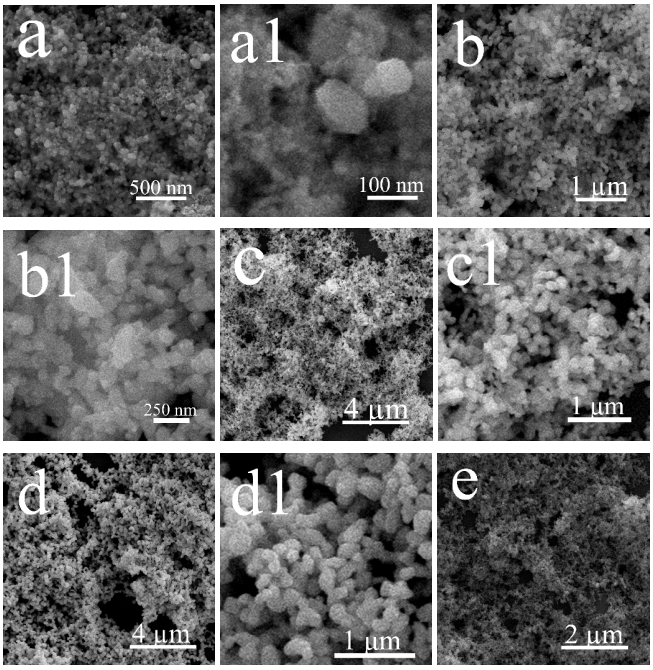

Fig. 3 SEM images of Ag/AgCl heterostructures. (a) Sample 2 with 10% AgCl. (b) Sample 3 with 30% AgCl. (c) Sample 4 with 50% AgCl. (d) Sample 7 with 80% AgCl. (e) Sample 9 with 100% AgCl. Their images with high magnification are shown in a1, b1, c1, and d1.

Fig. 3 shows the SEM images of Ag/AgCl heterostructures. Compared with sample 1 (Ag), no long rod was observed in Ag/AgCl nano heterostructures even though in the case of a low AgCl ratio (e.g., 10%). This indicates the reaction of Ag^0 transferred into Ag^+ occurred quickly. Such reaction resulted in the destroying of rod structures and the formation of Ag/AgCl nano heterostructures. In the case of AgCl ratio of 10%, the sizes of the heterostructure are from several tens to 150 nm. With increasing the amount of AgCl, the size distribution became narrow. As a result, the Ag/AgCl heterostructures consisted of small particles for the formation of loose structures. The composition of the Ag/AgCl heterostructures was identified by energy dispersive spectroscopy (EDS) analysis as shown in Fig. 4. The result indicates that the AgCl component is homogeneously distributed. This is ascribed to Ag particles with a loose structure.

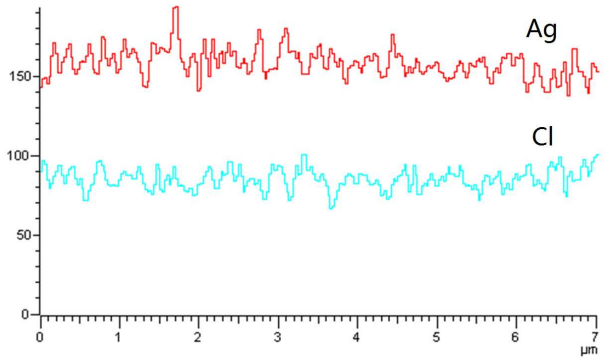

Fig. 4 Element distribution of line scanning via EDS line scanning analysis.

The formation mechanism of Ag/AgCl nano heterostructures was summarized to the transformation of Ag particles in situ. In the case of a low $FeCl_3$ ratio, inhomogeneous Ag/AgCl heterostructures formed as shown in Scheme 1 while molecularly homogeneous Ag/AgCl heterostructures were fabricated in the case of a large amount of $FeCl_3$. The size and morphologies of the heterostructures differs from those of Ag particles. Because of the difference of the lattice constant of AgCl (5.54 Å) and Ag (4.09 Å), the oxidation of Ag into Ag^+ resulted in crystalline stress which led to the reconstruction of monomers. The diffusion of reaction agents in loose Ag particles resulted in molecularly homogeneous nano heterostructures formed.

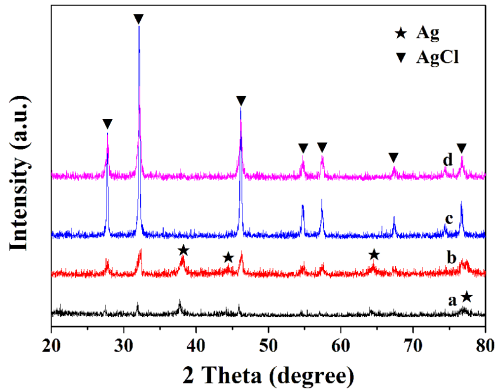

Fig. 5 XRD patterns of Ag/AgCl heterostructures. (a) Sample 2 with 10% of AgCl. (b) Sample 3 with 30% of AgCl. (c), Sample 4 with 50% of AgCl. (d) Sample 9 with 100% of AgCl.

To confirm the formation of Ag/AgCl heterostructures, Fig. 5 shows the XRD patterns of the heterostructures. The XRD peaks of samples consisted of Ag (JCPDS No.04-0783) and AgCl crystals (JCPDS No. 31-1238). No peaks from other crystal types are observed. With increasing the amount of $FeCl_3$, the intensity of the XRD peaks of the Ag crystals decreased gradually, whereas the intensity of the peaks of AgCl crystals increased significantly. This is confirmed the phase transfer between Ag and AgCl.

Fig. 6 shows the N_2-sorption isotherms and pore size distribution of samples 4 and 7. The corresponding nitrogen isotherm is of type III isotherms (BDDT classification). The analysis is the standard method for determining surface areas from nitrogen adsorption isotherms. The result suggests that the specific surface areas of

samples 4 and 7 are 20.5 and 19.7 m^2/g, respectively. The pore-size distribution is further confirmed by the corresponding pore-size distribution curve in the insets in Fig. 6. The pore size of samples 4 and 7 are 5.6 and 7.6 nm, respectively.

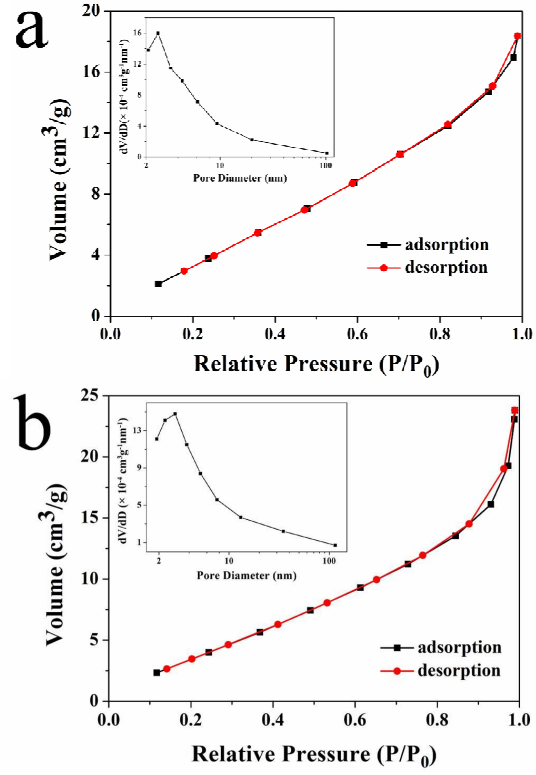

Fig. 6 N_2-sorption isotherms and pore size distribution of samples. (a) Sample 4. (b) Sample 7. Insets in (a) and (b) show the pore size distribution.

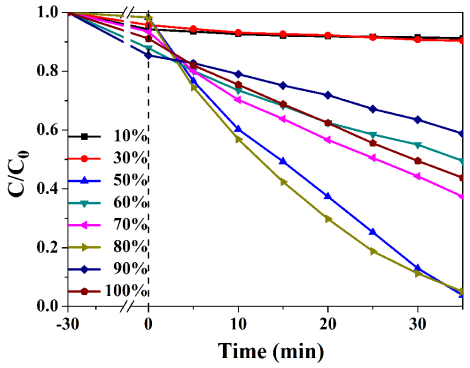

Fig. 7 Photocatalytic degradation profile of MO under UV light irradiation using Ag/AgCl nano heterostructures with different AgCl molar ratios.

The photocatalytic activity of Ag/AgCl heterostructures was evaluated by the degradation of MO under UV irradiation. Fig. 7 shows the degradation profiles of samples with different Ag/AgCl ratios. The area on the left of dashed line (negative value in X axis) represents the time used for adsorption-desorption equilibrium. The heterostructures revealed excellent photocatalytic activity when the molar ratios of AgCl are 50 and 80%. The reproducibility of experiments further confirmed this result. Although the mechanism for samples with AgCl of 50 and 80% is not clearly, this is mostly ascribed that the ratio of Ag and AgCl affect the separation of the photogenerated carriers. The enhanced photocatalytic behavior of the heterostructure is assigned to the efficient separation of the photogenerated carriers between the Ag and AgCl in the heterostructure.[17,19] The Fermi level of metallic Ag is lower than that of conduction band of the AgCl semiconductor,[5] facilitating the migration of photo-excited electrons to the metal surfaces. Such charge transfer divides electrons and holes into two distinct regions, and effectively suppresses the recombination of electronic-hole pairs. In addition, the electron migration to the metal surfaces also protects AgCl from photo-reduction, and makes it stable.[1]

As plotted in Fig. 7, C/C_0 and the reaction time (t) exhibits a linear relationship, indicating that the decomposition reaction of MO molecules follows the first-order kinetics.

$$-dC / dt = kC$$

where, C is the concentration of the MO molecules, C_0 is the initial concentration of the MO molecules, t is reaction time, and k is the rate constant. From results shown in Fig. 7, the rate constant is illustrated in Table 1. In the heterostructure, Ag works as electron trap and strongly absorbs light, whereas AgCl offers Cl for the degradation of MO molecules. The ratio of Ag and AgCl plays an important role for the photocatalytic activity of the nano heterostructures. In the case of low AgCl molar ratio, the heterostructure contained inhomogeneous Ag domains which affect the photolytic activity. With increasing the amount of AgCl, the heterostructure becomes molecularly homogeneous. In the cases of AgCl of 50 and 80%, the photogenerated electron–hole pairs were separated efficiently. Furthermore, the result from the investigation of N_2 adsorption-desorption isotherms indicates that the heterostructure did not reveal a porous structure even though it is loose according to SEM observation. This result also supported the heterostructure with high photocatalytic activity. For porous AgCl/Ag nanostructures, the enhanced photocatalytic activity cannot be expected because the interconnected ligaments in the porous heterostructures may act as straight routes for the transportation of photogenerated electrons and holes.

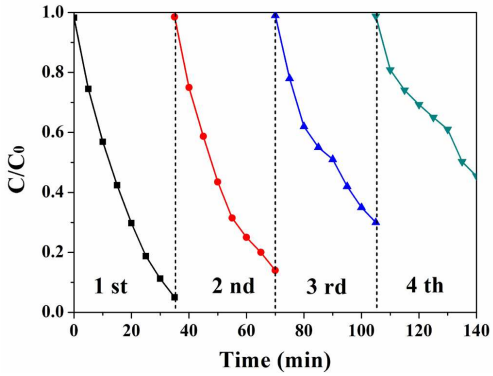

Fig. 8 Photostability performances of Ag/AgCl sample with AgCl molar ratio of 80% for degradation of MO under UV light irradiation.

To investigate the photostability of the Ag/AgCl sample for degradation of MO under UV and visible light irradiation, the sample was repeatedly used for 4 times after separation by centrifugation. Fig. 8 shows the photostability performances of Ag/AgCl sample with an AgCl molar ratio of 80% for degradation of MO upon UV light irradiation. At beginning, the adsorption occurred in dark. This is ascribed to the pore structure of samples. The photocatalytic performance of the sample continually decreased, and the degradation efficiency of MO was about 50% after 4 cycles. The decrease of the activity may be attributed to the photocorrosion

of the Ag/AgCl heterostructure under UV irradiation resulting from partial AgCl transformation into metallic silver.[20]

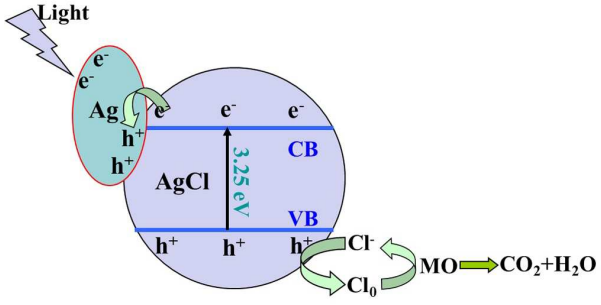

Scheme 2 Illustration of photocatalytic mechanism of molecularly homogeneous Ag/AgCl nano heterostructures.

An illustration of Ag/AgCl nano heterostructure formation and photocatalytic mechanism is depicted in Scheme 2. The Ag/AgCl nano heterostructures are highly photosensitive materials because of their composition. Molecularly homogeneous heterostructures make the separation of electrons and holes easily. Photons were firstly adsorbed by Ag and then photo-generated carriers were separated by AgCl to carry out the photodegradation of MO. Furthermore, the photo-generated electrons and holes arise from the dipolar character of the surface plasmon state of Ag molecules, which substantially increased the photocatalytic redox reaction.[19] These photo-generated electrons and holes were separated. Because holes were transferred to the surfaces of AgCl particles, Cl^- ions on the AgCl surfaces were oxidized to Cl^0 atoms, which enables to oxidize MO and hence reduced to Cl^- ions again. On the other, the electron transference to Ag surfaces prevents photo-reduction of AgCl.[19] Therefore, the Ag/AgCl nano-heterostructures exhibited good activity and stability.

Conclusions

Molecularly homogeneous Ag/AgCl nano heterostructures have been fabricated by a facile and novel two-step synthesis. Ag particles were prepared in ethanol using $AgNO_3$ and NaOH. The molar ratio of Ag and AgCl can be easily adjusted by changing the amount of $FeCl_3$. The heterostructures with AgCl ratios of 50 and 80% revealed excellent performance for the photocatalytic degradation of MO molecules. Because of high yield, facile route, and ideal properties, this rational synthetic route at room-temperature may be easily extended to fabricate other photocatalytic nano heterostructures and applied in some fields such as electronics, sensing, photonics and catalysis.

This work was supported in part by the project from National Research Program of China (973 Program, 2013CB632401), the program for Taishan Scholars, the projects from National Natural Science Foundation of China (51202090) and Outstanding Young Scientists Foundation Grant of Shandong Province (BS2012CL004 and BS2012CL006), and Graduate Innovation Foundation of University of Jinan, GIFUJN YCXZ13001.

Notes and references

[a]* School of Material Science and Engineering, University of Jinan, Jinan, 250022, P.R. China. E-mail: mse_yangp@ujn.edu.cn.

[b] Faculty of Chemical Engineering and Technology, Cracow University of Technology, Krakow, 31-155, Poland

1 C. An, S. Peng and Y. Sun, Adv. Mater. 2010, **22**, 2570.
2 Y. Tang, Z. Jiang, G. Xing, A. Li , P. D. Kanhere, Y. Zhang, T. C. Sum, S. Li, X. Chen, Z. Dong and Z. Chen, Adv. Funct. Mater. 2013, **23**, 2932.
3 L. Ye, J. Liu, C. Gong, L. Tian, T. Peng and L. Zan, ACS Catal. 2012, **2**, 1677.
4 P. Wang, B. Huang, X. Qin, X. Zhang, Y. Dai, J. Wei, M. H. Whangbo, Angew. Chem. Int. Ed. 2008, **47**, 7931.
5 M. Choi, K.-H. Shin, J. Jang, J. Colloid Interface Sci. 2010, 341, 83.
6 Y. Bi and J. Ye, Chem. Commun., 2010, **46**, 1532.
7 P. Wang, B. B. Huang, X. Y. Zhang, X. Y. Qin, H. Jin, Y. Dai, Z. Y. Wang, J. Y. Wei, J. Zhan, S. Y. Wang, J. P. Wang, M. H. Whangbo, Chem. Eur. J. 2009, **15**, 1821.
8 P. Wang, B. Huang, Z. Lou, X. Zhang, X. Qin, Y. Dai, Z. Zheng, X. Wang, Chem. Eur. J. 2010, **16**, 538.
9 L. Ai, C. Zhang and J. Jiang, Applied Catalysis B: Environmental 2013, **142– 143**, 744.
10 H. Xu, H. Li, J. Xia, S. Yin, Z. Luo, L. Liu and L. Xu, ACS Appl. Mater. Interfaces 2011. **3**. 22.
11 M. Zhu, P. Chen, W. Ma, B. Lei and M.a Liu, ACS Appl. Mater. Interfaces 2012, **4**, 6386.
12 M. Zhu, P. Chen and M. Liu, J. Mater. Chem., 2012, **22**, 21487.
13 M. S. Zhu, P. L. Chen, W. H. Ma, B. Lei and M. H. Liu, ACS Appl. Mater. Inter. 2012, **4**, 6386.
14 L. Han, P. Wang, C. Z. Zhu, Y. M. Zhai and S. J. Dong, Nanoscale 2011, **3**, 2931.
15 M. S. Zhu, P. L. Chen and M. H. Liu, Langmuir 2013, **29**, 9259.
16 G. Wang, H. Mitomo, Y. Matsuo, N. Shimamoto, K. Niikura, K. Ijiro, J. Mater. Chem. B, 2013, **1,** 5899
17 P. Hu, Y. Cao, Dalton Trans. 2012, **41**, 8908
18 C. Jia, P. Yang, B. Huang, ChemCatChem, 2014, **6**, 611.
19 J. T. Tang, Y. H. Liu, H. Z. Li, Z. Tan, D. T. Li, Chem. Commun. 2013, **49**, 5498.
20 C. L. Yu, G. Li, S. Kumar, K. Yang, R. C. Jin, Adv. Mater. 2014, **26**, 892.